Robust Magnetic/Polymer Hybrid Nanoparticles Designed for Crude Oil Entrapment and Recovery in Aqueous Environments

Adriana Pavía-Sanders,[†] Shiyi Zhang,[†,‡] Jeniree A. Flores,[†] Jonathan E. Sanders,[§] Jeffery E. Raymond,[†] and Karen L. Wooley[†,*]

[†]Department of Chemistry, Department of Chemical Engineering, and Laboratory for Synthetic-Biologic Interactions, Texas A&M University, P.O. Box 30012, 3255 TAMU, College Station, Texas 77842, United States, [‡]Department of Chemistry, Washington University in St. Louis, St. Louis, Missouri 63130, United States, and [§]Department of Civil Engineering, Texas A&M University, 3136 TAMU, College Station, Texas 77843, United States

ABSTRACT Well-defined, magnetic shell cross-linked knedel-like nanoparticles (MSCKs) with hydrodynamic diameters *ca.* 70 nm were constructed through the co-assembly of amphiphilic block copolymers of PAA_{20}-*b*-PS_{280} and oleic acid-stabilized magnetic iron oxide nanoparticles using tetrahydrofuran, *N*,*N*-dimethylformamide, and water, ultimately transitioning to a fully aqueous system. These hybrid nanomaterials were designed for application as sequestering agents for hydrocarbons present in crude oil, based upon their combination of amphiphilic organic domains, for aqueous solution dispersibility and capture of hydrophobic guest molecules, with inorganic core particles for magnetic responsivity. The employment of these MSCKs in a contaminated aqueous environment resulted in the successful removal of the hydrophobic contaminants at a ratio of 10 mg of oil per 1 mg of MSCK. Once loaded, the crude oil-sorbed nanoparticles were easily isolated *via* the introduction of an external magnetic field. The recovery and reusability of these MSCKs were also investigated. These results suggest that deployment of hybrid nanocomposites, such as these, could aid in environmental remediation efforts, including at oil spill sites, in particular, following the bulk recovery phase.

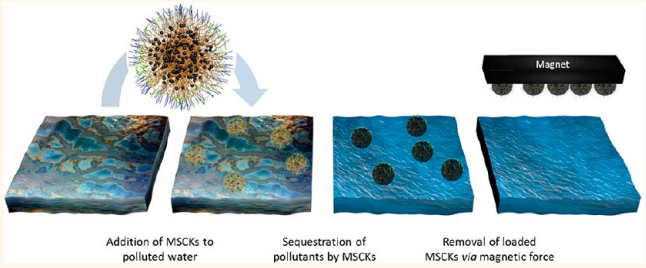

KEYWORDS: hybrid organic–inorganic nanoparticles · magnetic nanoparticles · oil recovery

Petroleum and other oils are an essential part of our society and daily lives; however, they also pose contamination problems. Notably, over 20 000 oil spills are reported to the U.S. government each year.[1] Although the severity of these cases varies widely, the effects of oil spills in the environment are permeating, as demonstrated recently by the Deepwater Horizon spill in the Gulf of Mexico.[2,3] Moreover, unwanted release of hydrocarbons during its extraction, processing, and distribution contributes to additional sources requiring remediation. During the initial stages of large-scale oil spill remediation from water, standard practices of collection and containment, such as booms, skimmers, and removal through suction, are effective for high levels of oil present. After this initial bulk recovery stage, low oil concentration in the aqueous environment appears as sheen of 0.04–50 μm thickness on the surface of the water.[4] Sorbent materials and bioremediation are often used for the removal of this residual oil; however, these techniques are often impractical, due to cost, time, and feasibility constraints.[3,5]

In recent years, innovative nanotechnology approaches have been developed to address oil spill remediation. For instance, much research has been performed in the development of nanomaterials for oil–water separation, from hydrogels,[6–8] sponges,[9–11] nanowires,[12,13] and nanoparticles,[14,15] among other materials.[16] Of particular interest are magnetic nanocomposites,[17] because the added magnetic component allows for recovery of the deployed nanomaterials. Predominantly, hydrophobic, magnetic materials have been studied for pollutant

* Address correspondence to wooley@chem.tamu.edu.

Received for review March 28, 2013 and accepted August 26, 2013.

Published online August 29, 2013
10.1021/nn401541e

© 2013 American Chemical Society

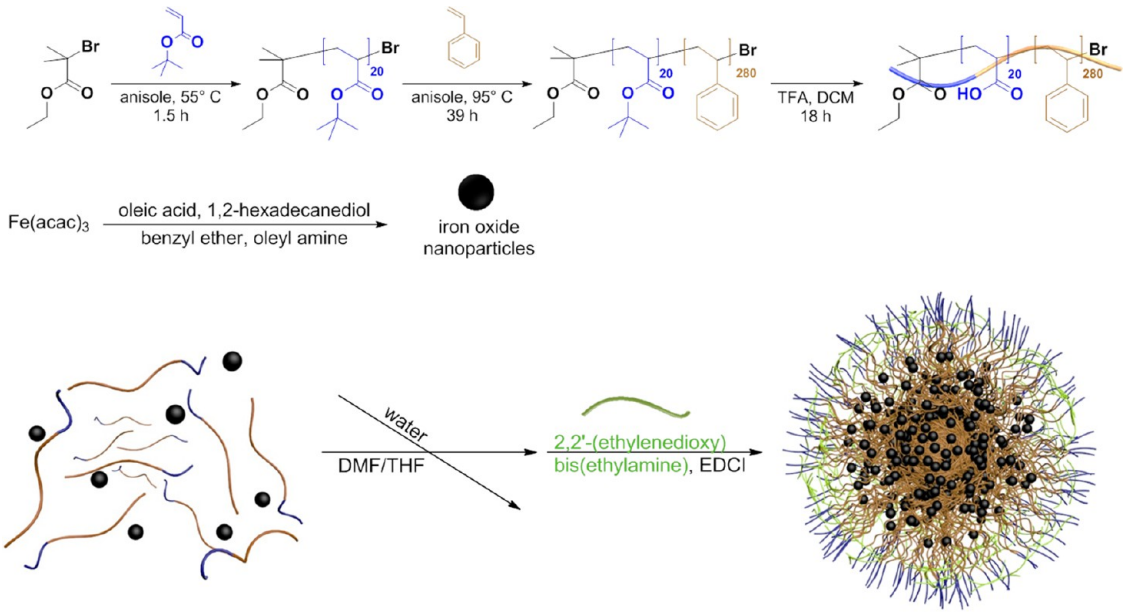

Scheme 1. Schematic representation of the construction of magnetic shell cross-linked (MSCK) nanoparticles.

recovery in aqueous environments, largely due to advances in hydrophobic and superhydrophobic materials and surfaces.[18,19] Calcagnile *et al.* have recently shown the successful removal of mineral oil from the surface of an aqueous solution by using a modified polyurethane foam, infused with iron oxide nanoparticles and functionalized with superhydrophobic polytetrafluoroethylene microparticles.[10] Similarly, highly hydrophobic hybrid nanoparticles coated with vinyl triethoxysilane have also proven to be an efficient method for oil separation and removal, as demonstrated by Zhu *et al.*[15] Although these materials were shown to selectively absorb hydrophobic pollutants in aqueous environments, experiments have been conducted against contaminants of limited complexity, such as lubricating oil, mineral oil, and other homogeneous oils, without the broad range of components that would be experienced in a crude oil spill.[6,9,10] Although the hydrophobic nature of these materials provide sequestration advantage, these materials neglect a crucial issue found at many spill sites, submerged oil. This particular problem continues to cause great strife, for instance, recently at the Kalamazoo River oil spill of 2010.[20] The use of amphiphilic materials is expected to be able to benefit the recovery of submerged oil and oils of varying densities, as they could traverse along the entire water column of a system. However, few well-defined, amphiphilic, hybrid materials have been investigated for pollutant entrapment and recovery. Perhaps the most intricately designed amphiphilic pollutant recovery vessel is the mesoporous silica-coated iron oxide nanoparticle system having small molecule surfactant-based micelles confined within the silica pores, which was shown to exhibit high hydrocarbon capture efficiencies, but with a limited capacity of 3.9 mg hydrocarbon/g nanoparticle material.[21] We anticipated that a hybrid nanomaterial that comprises inorganic magnetic nanoparticles and amphiphilic polymer layers would possess increased capacity for hydrocarbon pollutant packaging while maintaining aqueous phase dispersion stability and magnetic recovery properties. Moreover, to practically demonstrate that nanotechnology has a place in oil spill cleanup, we tested the materials presented here against a complex crude oil pollutant provided by Enbridge Energy Partners, L.P. (Figure S1).

RESULTS AND DISCUSSION

Design of MSCKs. To design novel materials for oil sequestering based on state-of-the-art nanotechnology, we first assessed the needs and requirements to deal with this type of environmental pollutant. The organic–inorganic hybrid, core–shell nanoparticles were specifically designed, as shown in Scheme 1, for oil extraction. The inorganic magnetic component was incorporated for a means of convenient recovery in an aqueous environment. Iron oxide nanoparticles were chosen, instead of *e.g.* nickel or cobalt magnetic nanoparticles, due to their lower potential of toxicity.[22,23] For the organic component, amphiphilic poly(acrylic acid)-*block*-polystyrene (PAA-*b*-PS) diblock copolymer was selected for the chemical stability of its backbone, the chemical reactivity of its side chain functionalities, and its ability to self-assemble into different morphologies.[24,25] The system was further cross-linked not only to protect it from disassembly during infinite dilution in the aqueous environment for which it was designed, but also to increase its loading potential by creating a stable vessel that could undergo reversible expansion and contraction. The self-assembly process

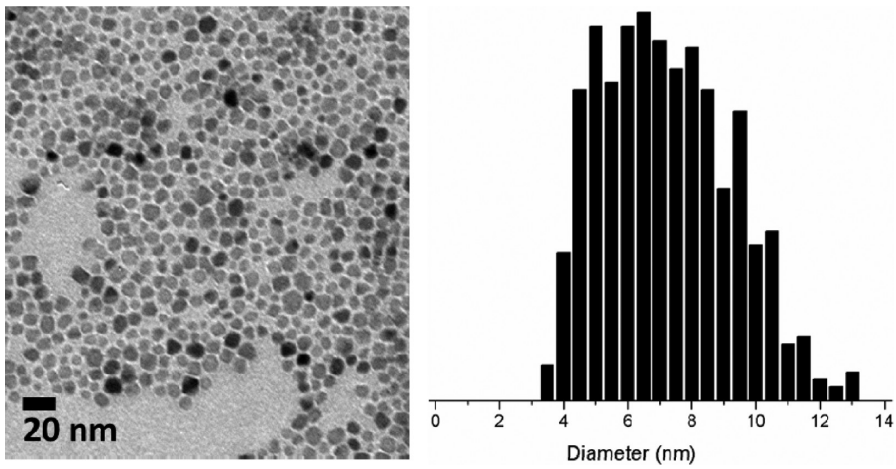

Figure 1. Characterization of iron oxide nanoparticles: (a) transmission electron microscopy (TEM) of iron oxide nanoparticles; (b) histogram of iron oxide nanoparticle population showing average diameter of 8 ± 2 nm.

we adopted here provided a large number of magnetic nanoparticles to be noncovalently incorporated within each hybrid nanoparticle core. Multiple, small nanoparticles in the same hybrid nanostructure enable core swelling during pollutant entrapment as this inorganic component is not covalently bound to the organic polymer and also increase the magnetic response of the material. Crude oil contains both aliphatic and aromatic fractions; the styrene groups within the PS-based core targets the aromatic components, while the backbone of the polymer allows for the increased solubility of the aliphatic fraction.

Thermal Synthesis of Iron Oxide Nanoparticles. Synthesis of iron oxide nanoparticles was conducted by following the thermal decomposition method.[26,27] Oleic acid and oleylamine were used as the surfactant and co-surfactant, respectively, in benzyl ether as the solvent, while 1,2-hexadecanediol served as a reducing agent for the iron(III) acetylacetonate. The reaction was conducted in three 1-h periods at temperatures of 140, 200, and 250 °C, consecutively. The resulting nanoparticles were precipitated in ethanol and characterized by transmission electron microscopy (TEM), superconducting quantum interference device (SQUID), and infrared (IR) spectroscopy. TEM showed nanoparticles of 8 ± 2 nm diameter (after analysis of over 100 nanoparticles) (Figure 1). SQUID confirmed the magnetic character and determined the particle size to be 9.2 nm, in agreement with the TEM data.

Synthesis of Amphiphilic Block Copolymer. The amphiphilic diblock copolymer PAA_{20}-*b*-PS_{280} was synthesized according to conditions previously reported.[28] In brief, sequential atom transfer radical polymerizations (ATRP) of *tert*-butyl acrylate and styrene were conducted in anisole in the presence of CuBr and *N*,*N*,*N*′,*N*′,*N*″-pentamethyldiethylenetriamine (PMDETA) at 55 and 95 °C, respectively, to afford a diblock copolymer precursor. The polydispersity indices (PDI) of the initial poly(*tert*-butyl acrylate)$_{20}$ homopolymer and the subsequent poly(*tert*-butyl acrylate)$_{20}$-*block*-polystyrene$_{280}$ diblock copolymer were below 1.2 (Figure S2). The final PAA_{20}-*b*-PS_{280} amphiphilic block copolymer was produced by subsequent removal of the *tert*-butyl groups through acidolysis with the aid of trifluoroacetic acid (TFA) in dichloromethane. Full characterization data for the polymers can be found in the Materials and Methods.

Co-Assembly of Hybrid Micelles. The co-assembly of the amphiphilic diblock copolymers and hydrophobic magnetic nanoparticles was performed by a modified process of a previously established method.[29] Magneto-micelles were chosen over other hybrid morphologies, such as magneto-polymersomes and magneto-core shell assemblies, due to their higher uniformity.[30] The PAA:PS mole ratio was tuned to 20:280 for its selectivity toward micellar structures; increasing this ratio results in a morphological change from magneto-micelles to magneto-polymersomes.[30] The PAA_{20}-*b*-PS_{280} and iron oxide nanoparticles were dissolved into a solvent mixture (vol ratio 1:1) of *N*,*N*-dimethylformamide (DMF) and tetrahydrofuran (THF) at a concentration of 0.33 mg/mL for both inorganic and organic components. The mixture was added dropwise, coincidentally with 1× volume of water, *via* two separate syringe pumps at 20 mL/h, into a vessel containing an initial 0.33× volume of nanopure water (a selective solvent for PAA) to afford the desired magnet containing block copolymer micelles. Finally, the excess organic solvents were removed by extensive dialysis (tubing having MWCO 6−8 kDa) against nanopure water for 24 h. The resulting nanoparticles were characterized by TEM, dynamic light scattering (DLS), and IR spectroscopy. TEM analysis showed nanoparticles of 70 ± 12 nm diameter (after counting over 35 micelles). Within the core of these structures, multiple iron oxide nanoparticles were observed (average of 75 after counting over 20 micelles; this average number is considered to be a lower limit, due to the two-dimensionality of

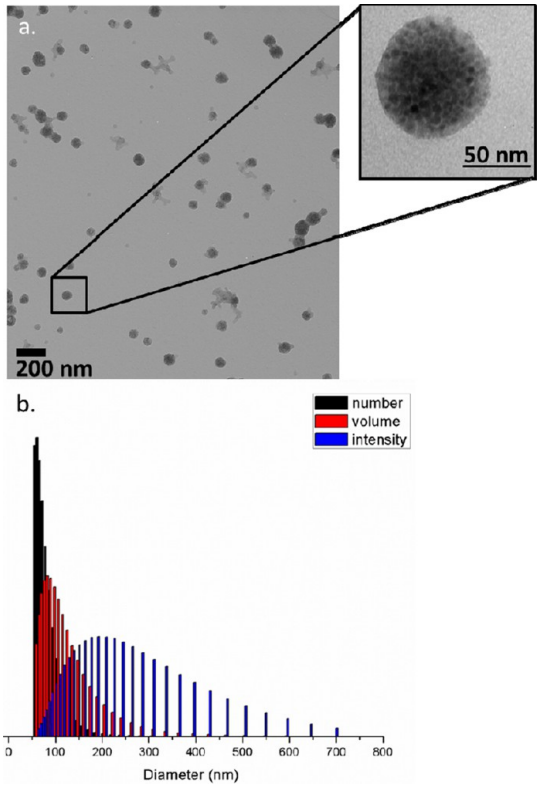

Figure 2. Characterization of magnetic iron oxide nanoparticles entrapped within PAA_{20}-*b*-PS_{280} MSCKs: (a) TEM of MSCKs drop deposited from water onto a Formvar grid (not stained); (b) number-, volume-, and intensity-averaged DLS histograms of MSCKs in water.

TEM creating difficulty to observe all iron oxide nanoparticles within a micellar assembly) (Figure S3). The packaging of the iron oxide nanoparticles within the core of the MSCKs was confirmed by tomographic TEM studies, as illustrated in a series of still and video images in the Supporting Information (Figure S4).

Cross-Linking of Hybrid Micelles *via* Amidation. The MSCKs were obtained by cross-linking nominally 25% of the acrylic acid repeat units by amidation with the amine groups of the cross-linker (2,2′-ethylenedioxy)-bis(ethylamine) in the presence of 1-(3-(dimethylamino)propyl)-3-ethyl-carbodiimide methiodide (EDCI). Extensive dialysis against nanopure water was performed to remove unreacted small molecules and reaction byproducts. The MSCKs were characterized by TEM (Figure 2a), atomic force microscopy (AFM) (Figure S5), DLS (Figure 2b), and IR spectroscopy. TEM imaging of the MSCKs demonstrated no morphological change after cross-linking. DLS and TEM confirmed no significant size difference post modification. In contrast to the micelles, the MSCKs were structurally more robust, which allowed for sample preparation and AFM imaging to be conducted. Although deposition onto mica resulted in imaging difficulties, due to AFM tip disruptions of particle placements on the substrate and destruction of particle integrity, sample deposition onto glass provided adequate AFM images of the MSCKs, which showed nanoparticles having an average diameter of 109 ± 50 nm and an average height of 3 ± 1 nm (after counting over 30 nanoparticles). This observation of a substantially greater diameter than height, together with the diameter being much larger when measured by AFM than by TEM or DLS, is characteristic of deformation of the particles when deposited onto the substrate used for AFM and/or during the AFM imaging procedure.[24,31] Moreover, it was observed that the particles were distributed across the glass substrate within a layer of other, unknown soft material, which resulted in an inaccurately low value for the measured heights of the MSCKs. However, the combined TEM, DLS and AFM data provided determination of the particle size and shape, and the interesting extents of particle deformation on the substrates are being investigated further to probe the roles that the magnetic particles may be able to play on responsive morphology and shape changes for these types of MSCKs. The IR C═O stretch at 1720 cm^{-1} in the magneto-micelle sample shifted upon amidation, and stretching bands at 1650 and 1560 cm^{-1} were observed for the MSCKs, which indicated successful cross-linking (Figure S6).[32]

Oil Sequestration by MSCKs. The ability of the MSCKs to serve as hybrid organic-magnetic sequestration vessels for oil spill recovery was assessed through a series of qualitative observations. The crude oil from the Texas-Oklahoma Enbridge pipeline was first weathered according to the method employed in experiments that investigated the Deepwater Horizon spill in the Gulf of Mexico.[33] The weathered oil (Figure S1) was added to deionized (DI) water in order to mimic contaminated water samples (Figure 3a) in 50 mL capped vials. The lyophilized powder samples of MSCKs were then added to the crude oil contaminated water at initial MSCK/oil weight ratios of 1:2, 1:5, 1:10, and 1:15. Visually, the oil sequestering capabilities of the well-defined MSCK nanoparticles were apparent (Figure 3b). The floating MSCKs exhibited a noticeable change in color from light tan to black within seconds after addition into the contaminated environment. This color change was accompanied by aggregation of the MSCKs. The change in color and texture was thought to be an indicator of the sorbing of the hydrocarbon contaminants. The magnetic nanoparticles were then easily and quickly (in a matter of seconds) attracted to the external magnetic field of a neodymium magnet to allow for the decanting of the contaminated water (Figure 3c). The remaining hydrocarbon contaminants were analyzed after they were extracted from their aqueous environment with the use of chloroform (a favorable solvent for this type of light sweet crude oil).

Quantification of Oil Sequestration. The capacity for oil sequestration by MSCKs was further quantified by an analytical method. To quantify the oil sequestered by

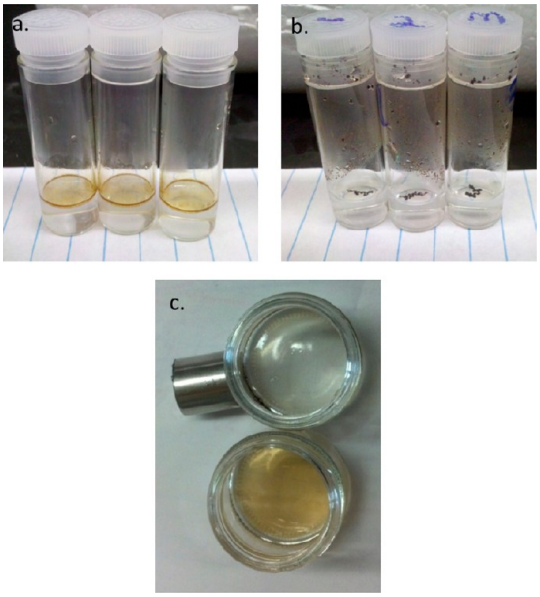

Figure 3. Images of oil sequestration experiment: (a) vial containing crude oil-contaminated water; (b) image showing vial after oil sorption by hybrid MSCK nanoparticles; (c) top view comparison of crude oil-loaded nanoparticles captured against the vial wall by an external magnet (top) and crude oil-contaminated water (bottom).

the MSCKs, the oil remaining in the aqueous phase after magnetic capture of the oil-sorbed MSCKs was extracted, analyzed and quantified using gel permeation chromatography (GPC). An internal standard of polystyrene (M_w= 70 000 Da) was used to spike each dilute oil sample prior to injection into the instrument. This high molecular weight polymer was selected for its short retention time; the crude oil chromatogram is broad and has a relatively high retention time due to the inherently small to medium molecular weights of the crude oil components.

A refractive index (RI) detector was used as a concentration detector in a GPC system according to the RI detector theory.[34] Quantification of the oil recovery was made possible due to the proportionality between sample concentration and refractive indices. Several examples of this applied theory have been used to determine polymer concentration in both cyclic and linear systems.[35−37] Though this method is effective in more homogeneous systems, the heterogeneity of the crude oil sample led to complications during the development of this procedure. To compensate for this, a control group of "unrecovered" oil was used as a baseline for the oil quantification method. These control groups were used to derive an empirical coefficient relating the oil concentration in the sample to the integration region in the chromatogram for each set of experiments. This coefficient was later employed to determine the unknown oil concentration remaining after MSCK sequestration in the tested samples. Further details of this methodology can be found in the materials and methods.

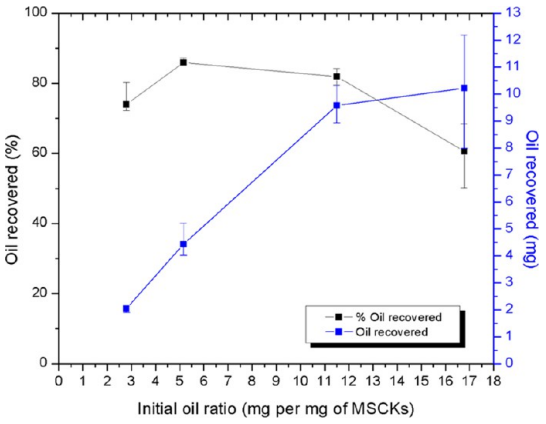

Figure 4. Oil recovery data: percentage recovery in black, mass recovered in blue.

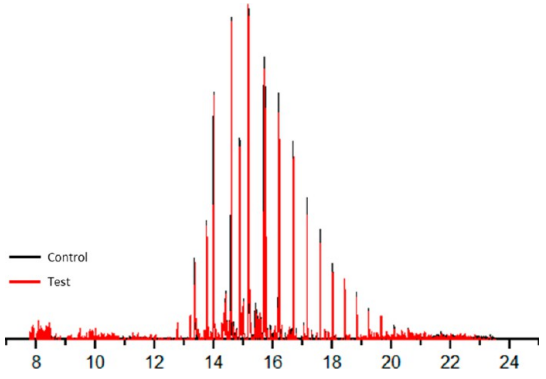

Figure 5. Gas chromatography−mass spectrometry (GC-MS) of oil extracted from control (black) and test (red) groups.

The maximum sorption capacity of the MSCKs was determined by testing increasing initial nanoparticle: oil ratios through a series of experiments. For the initial ratio of 1:2.8, evaluation of the chromatographical data determined the total oil sorption to be 2.1 mg of oil/mg of MSCKs used. For the remaining trials of 1:5.2, 1:11.5, and 1:16.8, the sorption limit was found to be 1:4.4, 1:9.6, and 1:10.2, respectively. The percentage oil recovery was also determined (Figure 4). Following the trend seen in the mass recovery data on the graph below, it can be speculated that the maximum sorption extent of the MSCKs is roughly ten times the initial dry weight of the material. Further attempts at increasing initial oil concentration resulted in inadequate recovery of the loaded nanoparticles; at higher oil concentrations, the viscosity of the thick oil layer prevented magnetic mobilization of the loaded nanoparticles.

Gas chromatography−mass spectrometry (GC-MS) was used to perform a qualitative comparison of the weathered crude oil and the oil extracted from the testing groups. The data from this test showed the successful sequestration of all oil components by MSCKs (Figure 5), without any fractionation of the oil materials. This result suggests that fine-tuning of the

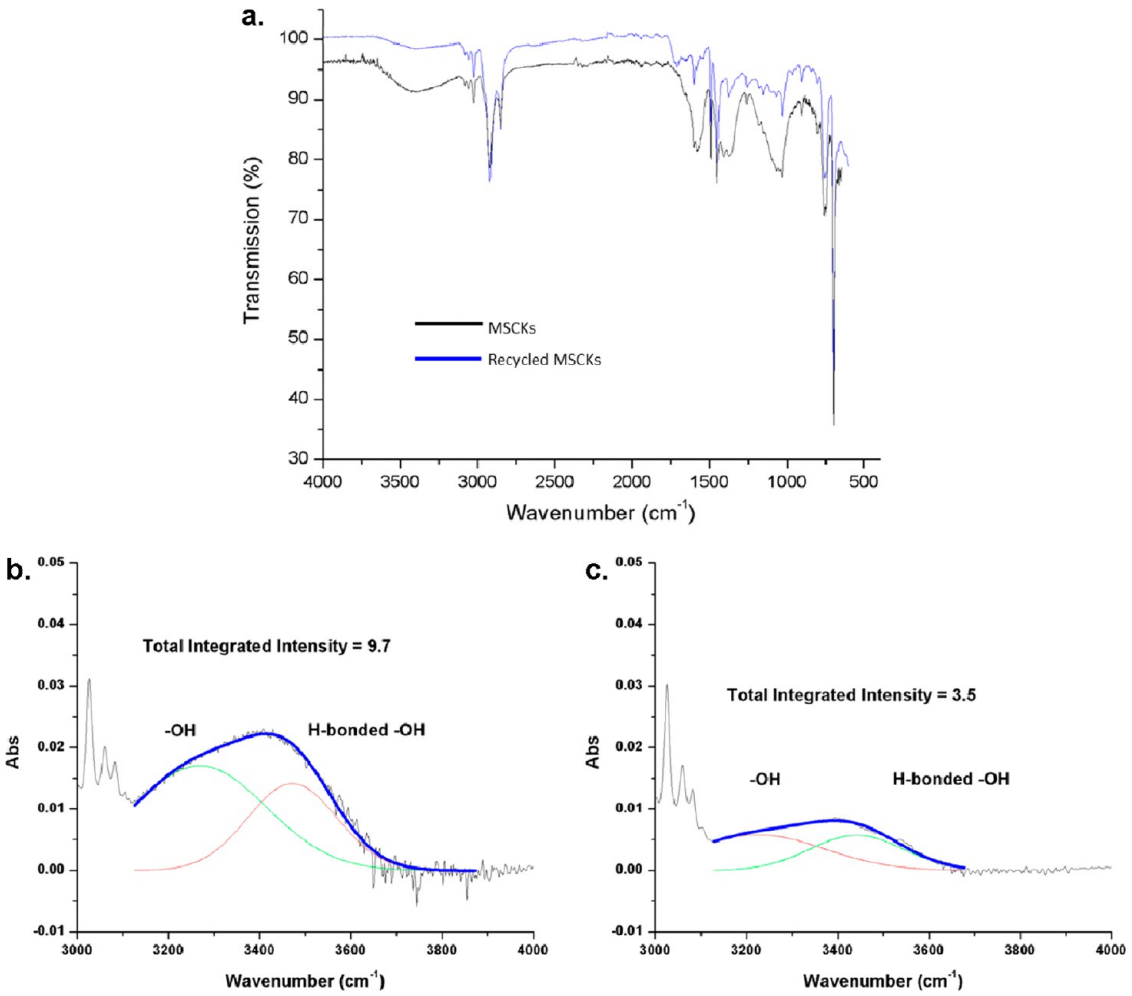

Figure 6. (a) IR spectra of pristine and recycled MSCKs. (b) Quantification of −OH functionality of pristine MSCKs. (c) Quantification of −OH functionality of recycled MSCKs.

organic component of the MSCK system could achieve selective recovery of a broad range of environmental pollutants, coincidentally, which may be useful for various applications.

Recycling of MSCKs. The reuse of materials at oil spill sites decreases the waste produced during the cleanup efforts as well as enhances the overall effectiveness of the substance deployed. Other magnetic systems have been successfully recycled and re-deployed as recovery systems for environmental pollutants.[21] The magnetic permanently confined micelle arrays used by Wang *et al.* were tested for their recyclability and were regenerated after thorough washings in methanol.[21] Solubility analysis of the crude oil determined that ethanol, rather than methanol, would be the better solvent suited for our particular crude oil system. Although chloroform could have also been used for the removal of the oil from the MSCK system, there were initial concerns regarding chloroform promoting morphological changes of the nanoparticles.

The oil sorbed in the nanoparticles was removed by extensive washings in ethanol with the help of sonication. The contaminated ethanol was decanted between each washing and the nanoparticles were retained in the vessel through magnetic force. Visually, the "clean" nanoparticles returned to their original light tan color. After *in vacuo* drying, IR spectroscopy was used to determine the state of the MSCKs (Figure 6a). As seen on the IR spectra of the pristine and recycled MSCKs, there were some observable changes after the washing procedure, in particular between 1700 and 800 cm^{-1}. We hypothesize these may be due to reorganization of the polymeric structures during the sonication washes; ongoing efforts include determining the molecular compositional origins of these changes. An additional aspect of the IR spectra that was further investigated was the apparent loss of −OH functionality after the removal of the oil from the loaded MSCKs. Quantification of this loss was performed through the analysis of the IR absorption spectra by first normalizing the two data sets using a peak in which change did not occur, the C−H band of the polymer backbone at 1450 cm^{-1}. The data from this analysis as shown in Figure 6b,c demonstrate a 40% loss of the −OH functionality, presumably from dehydration and esterification of the acrylic acid

groups in the polymer component of the MSCK system. Further detailed studies of the recycling method, with full mass analyses of the recovered hydrocarbon and MSCKs, are underway to demonstrate that this loss was not artificially enhanced by the presence of remaining hydrocarbons. However, alcohol washing of pristine, lyophilized MSCK nanoparticles with sonication also resulted in a reduction in the intensity of the −OH signal after analysis of the deconvoluted data, likely due to esterification of intermediate anhydrides. We believe that the anhydride moieties are formed during the freeze-drying process to obtain the powder MSCKs and/or during sonication. The presence of these anhydrides can be observed at 1000 cm^{-1} in Figure S7.

Although further investigations into the changes experienced by the MSCKs after washing are ongoing, the recycled nanoparticles were redeployed into a polluted aqueous system with an initial MSCK/oil ratio of 1:15.7 to probe the reusability of these materials. After oil sequestration and analysis of remaining pollutants, the sorption ratio was calculated to be 1:10.9. These data were compared to those of the previous 1:15 initial ratio experiment where the oil sorption was calculated to be 1:10.2, demonstrating retention of their ultrahigh oil sorption characteristics. This finding addresses a challenge associated with the efficiency and effectiveness of this material in a real-world application.

CONCLUSIONS

MSCKs for removal of environmental pollutants have been prepared and their loading capabilities were determined. These well-defined nanoparticles showed efficient oil sorption capacity of 10-fold their initial dry weight when introduced into an aqueous environment polluted with a complex crude oil. Compared to materials that are typically employed in the field currently, which have capacities of *ca.* 4-fold oil uptake to their dry mass, MSCKs offer distinct improvement.[38] Moreover, the recyclability of the robust MSCK material was also proven to be highly effective, despite some apparent chemical changes experienced during the recycling process. Furthermore, this type of material has high potential for additional applications in environmental remediation. The amphiphilic nature of the MSCK system expands the potential use of these materials to other applications such as the removal of submerged oil, groundwater remediation, and cleanup of contaminated soils. Modern advances in polymer science hold the promise of fine-tuning the complex composition of the polymer components, for a more targeted design to meet the demands of particular applications.

MATERIALS AND METHODS

Materials. All chemicals were purchased from Aldrich Chemical Co. and used without further purification unless otherwise noted. *tert*-Butyl acrylate and styrene monomers were purified through an alumina plug to remove stabilizer. Iron(III) acetylacetonate was purchased from Strem Chemicals, Inc. Nanopure water (18 MΩ·cm) was acquired by means of a Milli-Q water filtration system, Millipore Corp. (Bedford, MA). Neodymium magnet (90 lb pull) was purchased from magnets4less.com. Crude oil for this research was generously donated by Enbridge Energy Partners, L.P.

Characterization Techniques. ^{1}H NMR and ^{13}C NMR spectra were recorded on an Inova 300 or Mercury 300 spectrometer interfaced to a UNIX computer using VnmrJ software. Samples were prepared as solutions in $CDCl_3$ or THF-d_8 and solvent protons were used as internal standard. IR spectra were recorded on an IR Prestige 21 system (Shimadzu Corp., Japan). A small amount of sample was placed to cover the ATR crystal for IR measurements. Data were analyzed using IRsolution software. Differential scanning calorimetry studies were performed on a Mettler Toledo DSC822 (Mettler-Toledo, Inc., Columbus, OH) calibrated according to the standard procedures using indium. The heating rates were 10 °C min^{-1} and cooling rates were 10 °C min^{-1} with a temperature range of −100 to 150 °C. The T_g was taken as the midpoint of the inflection tangent, upon the third heating scan. Thermogravimetric analysis was performed under Ar atmosphere using a Mettler Toledo model TGA/DSC1 with a heating rate of 10 °C/min. Measurements were analyzed using Mettler Toledo STAR^e software v 10.00. THF gel permeation chromatography (GPC) was conducted on a system equipped with Waters chromatography, Inc. (Milford, MA) model 1515 isocratic pump and a model 2414 differential refractometer with a three-column set of Polymer Laboratories, Inc. (Amherst, MA) Styragel columns (PL_{gel} 5 μm Mixed C, 500 Å, and 10^4 Å, 300 × 7.5 mm columns) and a guard column (PL_{gel} 5 μm, 50 × 7.5 mm). The system was equilibrated at 40 °C in THF, which served as the polymer solvent and eluent (flow rate set to 1.00 mL/min). The differential refractometer was calibrated with Polymer Laboratories, Inc., polystyrene standards (300−467 000 Da). Polymer solutions were prepared at a concentration of *ca.* 3 mg/mL with 0.05% vol toluene as flow rate marker and an injection volume of 200 μL was used. Data were analyzed using Empower Pro software from Waters Chromatography, Inc. Chloroform GPC for oil analysis was conducted on a system equipped with a Tosoh Corporation (Tokyo, Japan) model HLC-8320 EcoSEC system with a two-column set of TOSOH Bioscience TSKgel columns (Super HM-M 6.0 mm i.d. tme15 cm columns) and a guard column (Super H−H 4 μm). The system was equilibrated at 40 °C in chloroform, which served as the polymer solvent and eluent (flow rate set to 0.600 mL/min). The differential refractometer was calibrated with Polymer Laboratories, Inc., polystyrene standards (580−370 000 Da). Polymer solutions were prepared at a concentration of *ca.* 3 mg/mL and an injection volume of 200 μL was used. Dynamic light scattering (DLS) measurements were conducted using Delsa Nano C from Beckman Coulter, Inc. (Fullerton, CA) equipped with a laser diode operating at 658 nm. Size measurements were made in water ($n = 1.3329$, $\eta = 0.890$ cP at 25 ± 1 °C; $n = 1.3293$, $\eta = 0.547$ cP at 50 ± 1 °C; $n = 1.3255$, $\eta = 0.404$ cP at 70 ± 1 °C). Scattered light was detected at 165° angle and analyzed using a log correlator over 70 accumulations for a 0.5 mL of sample in a glass sizing cell (0.9 mL capacity). The photomultiplier aperture and the attenuator were automatically adjusted to obtain a photon counting rate of *ca.* 10 kcps. The calculations of the particle size distribution and distribution averages were performed using CONTIN particle size distribution analysis routines. Prior to analysis, the samples were filtered through a 0.45 μm Whatman nylon membrane filter (Whatman, Inc.). The samples in the glass sizing cell were equilibrated at the desired temperature for 5 min before measurements were made. The peak average of histograms from intensity, volume, or number distributions out of 70 accumulations was reported as the average diameter of the particles.

Synthesis of Poly(*tert*-butyl acrylate) ($PtBA_{20}$) *via* ATRP. A flame-dried 100-mL Schlenk flask equipped with a magnetic stir bar was charged with PMDETA (1 equiv, 451.0 mg, 2.6 mmol), *t*BA (30 equiv, 9.6322 g, 75.1 mmol), ethyl α-bromoisobutyrate (1 equiv, 489.5 mg, 2.5 mmol), and anisole (10 mL). The flask was sealed with a rubber septum and the reaction mixture was degassed by three freeze−pump−thaw cycles. Then, the CuBr (1 equiv, 430.5 mg, 4.2 mmol) was added under a nitrogen flow to the frozen mixture. Following two additional freeze−pump−thaw cycles, the reaction mixture was allowed to return to room temperature and to stir for 10 min to ensure homogeneous mixing. The flask was then immersed into a preheated oil bath at 55 °C to start the polymerization. The polymerization was monitored by analyzing aliquots collected at predetermined times by ^{1}H NMR spectroscopy. As the expected monomer conversion was reached, after *ca.* 1 h, the polymerization was quenched by quick immersion of the reaction flask into liquid N_2 and exposure to air. THF (20 mL) was added to the reaction flask and the polymer was purified by filtration through an alumina plug followed by subsequent precipitation into 500 mL of a methanol/ice mixture (3×). The precipitants were collected and dried under vacuum overnight to afford 3.62 g of $PtBA_{20}$ as a white solid, giving 40% yield of the 95% conversion polymerization. $M_{n(NMR)}$ = 3.1 kDa, $M_{n(GPC)}$ = 2.8 kDa, PDI = 1.09. IR: 2975, 2720, 1725, 1465, 1440, 1390, 1360, 1250, 845, 750 cm^{-1}. ^{1}H NMR (300 MHz, $CDCl_3$) δ 4.12 (q, *J* = 7 Hz, 2H), 2.35−2.15 (br, 20H), 1.94−1.78 (br, 10H), 1.71−1.2 (m, 210H), 1.27 (t, *J* = 7 Hz, 3H), 1.12 (br, 6H) ppm. ^{13}C NMR (75 MHz, $CDCl_3$) δ 27.8−28.2, 35.0−37.6, 41.4−42.5, 80.2−80.7, 173.8−174.4 ppm. DSC: T_g = 28 °C. TGA: T_{onset} = 195 °C. $T_{decomposition}$: (195−204 °C) 43.5% mass loss; (207−455 °C) 46.5% mass loss; 10% mass remaining.

Synthesis of Poly(*tert*-butyl acrylate)$_{20}$-*b*-polystyrene$_{280}$ ($PtBA_{20}$-*b*-PS_{280}) *via* ATRP. A flame-dried 25-mL Schlenk flask equipped with a magnetic stir bar was charged with PMDETA (1.6 equiv, 18.1 mg, 0.1 mmol), styrene (500 equiv, 3.1303 g, 30 mmol), $PtBA_{20}$ (1.3 equiv, 257.6 mg, 0.1 mmol), and anisole (4 mL). The flask was sealed with a rubber septum and the reaction mixture was degassed by three freeze−pump−thaw cycles. Then, the CuBr (1 equiv, 8.6 mg, 0.06 mmol) was added under a nitrogen flow to the frozen mixture. Following two more freeze−pump−thaw cycles, the reaction mixture was allowed to return to room temperature and to stir for 10 min to ensure homogeneous mixing. The flask was then immersed into a preheated oil bath at 95 °C to start the polymerization. The polymerization was monitored by analyzing aliquots collected at predetermined times by ^{1}H NMR spectroscopy. As the expected monomer conversion was reached, after *ca.* 39 h, the polymerization was quenched by quick immersion of the reaction flask into liquid N_2 and exposure to air. THF (5 mL) was added to the reaction flask and the polymer was purified through filtration by an alumina plug and precipitation into 200 mL of cold methanol (2×). The precipitants were collected and dried under vacuum overnight to afford $PtBA_{20}$-*b*-PS_{280} as an off-white solid, giving 64% yield of the 55% conversion polymerization. $M_{n(NMR)}$ = 31.7 kDa. $M_{n(GPC)}$ = 27.0 kDa. PDI = 1.18. IR: 3080, 3060, 3020, 2920, 2840, 1940, 1880, 1800, 1725, 1600, 1490, 1450, 1360, 1240, 1150, 1060, 1025, 910, 840, 750, 695 cm^{-1}. ^{1}H NMR (300 MHz, $CDCfl_3$) δ 7.43−6.8 (br, 840H), 6.8−6.13 (br, 560H), 4.12 (q, *J* = 7 Hz, 2H), 2.24−0.87 (br m, 1090H) ppm. ^{13}C NMR (75 MHz, $CDCl_3$) δ 27.8−28.2, 39.6−46.5, 80.2−80.7, 125.2−126.0, 127.0−128.4, 144.7−146.3, 173.8−174.4 ppm. DSC: T_g = 88 °C. TGA: T_{onset} = 237 °C. $T_{decomposition}$: (237−241 °C) 4% mass loss; (401−435 °C) 73.6% mass loss; 22% mass remaining.

Synthesis of Poly(acrylic acid)$_{20}$-*b*-polystyrene$_{280}$ (PAA_{20}-*b*-PS_{280}). $PtBA_{20}$-*b*-PS_{280} (1 mol equiv, 1.0666 g) was dissolved in dichloromethane (10 mL). Trifluoroacetic acid (TFA) (1000 mol equiv, 3 mL) was added. The reaction mixture was left stirring vigorously for 16 h. After evaporation of the solvent and TFA, THF was added to redissolve the polymer which was then dialyzed for three days against nanopure water using dialysis tubing having MWCO 6−8 kDa, during which the product precipitated within the dialysis tubing. The precipitate was filtered and placed under high vacuum overnight. IR: 3080, 3060, 3025, 3000, 2920, 2850, 1925, 1860, 1800, 1700, 1600, 1490, 1450, 1370, 1260, 1170, 1150, 1065, 1025, 900 750, 700 cm^{-1}. ^{1}H NMR (300 MHz, THF) δ 10.88 (br, 10H), 7.3−6.8 (br, 840H), 6.8−6.59 (br, 560H), 4.07 (q, *J* = 7 Hz, 2H), 2.47−0.48 (br m, 930H). ^{13}C NMR (75 MHz, THF) δ 40.0−46.7, 125.2−126.0, 127.0−128.4, 144.7−146.3, 173.8−174.4 ppm. DSC: T_g = 99 °C. TGA: T_{onset} = 410 °C. $T_{decomposition}$: (410−441 °C) 89.5% mass loss; 10.5% mass remaining.

Synthesis of Fe_3O_4 Nanoparticles. A flame-dried, 50 mL 3-neck flask equipped with a magnetic stir bar and condenser was charged with $Fe(acac)_3$ (1 mol equiv, 719.5 mg, 2 mmol), oleic acid (3 mol equiv, 2.3215 g, 6 mmol) and oleyl amine (3 mol equiv, 2.0020 g, 6 mmol). After the addition of benzyl ether (20 mL) and 1,2- hexadecanediol (5 mol equiv, 2.5808 g, 10 mmol), the reaction mixture was degassed by a three-cycle exposure to vacuum and nitrogen. The reaction temperature was taken to 140 °C and the pressure inside the reaction vessel was relieved by the insertion of a needle. After an hour, the needle was removed and the reaction temperature was taken to 200 °C for an additional hour, following an hour at 250 °C. Once the reaction mixture was cooled to room temperature, it was transferred into a centrifuge tube and the nanoparticles were precipitated by addition of EtOH (3×) and resuspended in THF. Final nanoparticle size was determined *via* TEM and DLS as *ca.* 8 nm in diameter. IR: 2600, 2220, 1220, 500, 450, 420 cm^{-1}. TGA: T_{onset} = 210 °C. $T_{decomposition}$: (210−270 °C) 3.5% mass loss, (300−430 °C) 11.5% mass loss; 88.5% mass remaining.

Co-Assembly of PAA_{20}-*b*-PS_{280} and Fe_3O_4 NPs. An organic solution containing 2 mL of a 10 mg/mL solution of PAA_{20}-*b*-PA_{280} in DMF was diluted with a mixture of 28.0 mL of DMF and 28.6 mL of THF. To this was added a 1.4 mL of a 14 mg/mL solution of iron oxide nanoparticles in a dropwise manner under stirring. The solution was allowed to stir vigorously for 30 min to ensure homogeneity. The 60 mL of organic solution was added dropwise to an initial 20 mL of nanopure water at a rate of 20 mL/h. Simultaneously, 60 mL of nanopure water was also added at the same rate. The resulting 70 nm micelles were cross-linked to nominally 25% based on acrylic acid units (1 mol equiv, 1.51 × 10^{-5} mol) with the aid of 2,2′-(ethylenedioxy)bis(ethylamine) (0.125 mol equiv, 1.89 × 10^{-6} mol, 0.224 mg) and 1-[3-(dimethylamino)propyl]-3-ethylcarbodiimide methiodide (EDCI) (0.275 mol equiv, 4.15 × 10^{-6} mol, 0.984 mg), assuming 80% polymer present after filtration through 5.0 μm filter. DLS, TEM, and AFM data were used to determine the size of the MSCKs to be 70 nm.

Representative Procedure for Oil Sequestration. To a vial containing DI water was added weathered crude oil originating from the Texas-Oklahoma pipeline (light sweet crude), and the weight of the sample was recorded. To each testing vial were added MSCKs in the form of powder (1−10 mg depending on scale of trial). After approximately 30 min with little to no agitation, the loaded MSCKs were attracted by an external magnetic field to allow for decantation of the oil contaminated water for oil extraction; the vial was washed three times with water to maximized removal of the oil/water mixture remaining. The oil was extracted using chloroform washings. The organic fraction containing the crude oil was spiked with a solution of polystyrene standard of 70 000 Da molecular weight to serve as an internal standard for comparative studies with the control group. The spiked samples were examined using a chloroform GPC. Oil recovery was determined by chromatogram comparison with data from the control group. Oil was also extracted from contaminated water in the control groups using chloroform. Experiments were conducted in triplicate.

Oil Quantification through GPC Analysis. To account for the behavior and RI response of the crude material through the column, the spiked samples from the control groups were analyzed through chloroform GPC. With the use of the known mass of oil present in the control samples, a relationship between the area under the chromatogram peak and oil mass was established (mathematically, this was accomplished through the use of coefficient *k*).

$$k \cdot \frac{\int_{soil}}{\int_{spike}} = \frac{M_{oil}}{M_{spike}}$$

The use of this coefficient was validated by the low percent variation of this number within a sample set (5−15%). This *k* value was subsequently used in the tested samples to determine the unknown oil mass in the samples (M_{oil}). A data sample can be observed in the table below where "T#" represents the testing groups, and "C#" the control groups.

sample	oil (mV·sec)	PS (mV·sec)	oil used (mg)	*k*
T1	235.679	270.429	15.9	
T2	93.488	151.1	17.8	
T3	48.255	71.898	16.6	
C1	589.425	340.313	15.4	2.877
C2	718.811	339.255	18.8	2.872
C3	558.667	329.665	116.3	3.075

Conflict of Interest: The authors declare no competing financial interest.

Acknowledgment. We gratefully acknowledge financial support from the National Science Foundation under grant number DMR-1105304, and the Welch Foundation through the W. T. Doherty-Welch Chair in Chemistry under grant number A-0001. Enbridge Energy Partners, L.P. is gratefully acknowledged for their generous donation of the West Texas crude oil, and we thank Dr. Hansoo Kim for the TEM tomography studies.

Supporting Information Available: Additional characterization data, including GC-MS chromatogram of weathered crude oil, GPC and IR data for the polymers, IR, TEM, TEM tomographic, and AFM data of the magneto-micelles and MSCKs. This material is available free of charge *via* the Internet at http://pubs.acs.org.

REFERENCES AND NOTES

1. Testimony of Lisa P. Jackson, Administrator U.S. Environmental Protection Agency, 2010. http://www.epa.gov/ocirpage/hearings/testimony/111_2009_2010/2010_0224_lpj.pdf.
2. White, H. K.; Hsing, P. Y.; Cho, W.; Shank, T. M.; Cordes, E. E.; Quattrini, A. M.; Nelson, R. K.; Camilli, R.; Demopoulos, A. W.; German, C. R.; *et al.* Impact of the Deepwater Horizon Oil Spill on a Deep-Water Coral Community in the Gulf of Mexico. *Proc. Natl. Acad. Sci. U.S.A.* **2012**, *109*, 20303–20308.
3. Barron, M. G. Ecological Impacts of the Deepwater Horizon Oil Spill: Implications for Immunotoxicity. *Toxicol. Pathol.* **2012**, *40*, 315–320.
4. Identification of Oil on Water: Aerial Observation and Identification Guide. Australian Maritime Safety Authority, 2009. http://www.amsa.gov.au/forms-and-publications/Publications/Oil_on_Water_April09.pdf.
5. Understanding Oil Spills and Oil Spill Response. In *Office of Emergency and Remedial Response*; U.S. Environmental Protection Agency: Washington, D.C.; **1999**. http://www4.nau.edu/itep/waste/HazSubMap/docs/OilSpill/EPAUnderstandingOilSpillsAndOilSpillResponse1999.pdf.
6. Cong, H.; Ren, X.; Wang, P.; Yu, S. Macroscopic Multifunctional Graphene-Based Hydrogels and Aerogels by a Metal Ion Induced Self-Assembly Process. *ACS Nano* **2012**, *6*, 2693–2703.
7. Korhonen, J. T.; Kettunen, M.; Ras, R. H.; Ikkala, O. Hydrophobic Nanocellulose Aerogels as Floating, Sustainable, Reusable, and Recyclable Oil Absorbents. *ACS Appl. Mater. Interfaces* **2011**, *3*, 1813–1816.
8. Basak, S.; Nanda, J.; Banerjee, A. A New Aromatic Amino Acid Based Organogel for Oil Spill Recovery. *J. Mater. Chem.* **2012**, *22*, 11658–11664.
9. Zhu, Q.; Pan, Q.; Liu, F. Facile Removal and Collection of Oils from Water Surfaces through Superhydrophobic and Superoleophilic Sponges. *J. Phys. Chem. C* **2011**, *115*, 17464–17470.
10. Calcagnile, P.; Fragouli, D.; Bayer, I. S.; Anyfantis, G. C.; Martiradonna, L.; Cozzoli, P. D.; Cingolani, R.; Athanassiou, A. Magnetically Driven Floating Foams for the Removal of Oil Contaminants from Water. *ACS Nano* **2012**, *6*, 5413–5419.
11. Gui, X.; Cao, A.; Wei, J.; Li, H.; Jia, Y.; Li, Z.; Fan, L.; Wang, K. Soft, Highly Conductive Nanotube Sponges and Composites with Controlled Compressibility. *ACS Nano* **2010**, *4*, 2320–2326.
12. Canter, N. More Efficient Cleanup of Oil Spills. *Tribol. Lubr. Technol.* **2008**, *64*, 12–13.
13. Yuan, J.; Liu, X.; Akbulut, O.; Hu, J.; Suib, S. L.; Kong, J.; Stellacci, F. Superwetting Nanowire Membranes for Selective Absorption. *Nat. Nanotechnol.* **2008**, *3*, 332–336.
14. Zhu, L.; Li, C.; Wang, J.; Zhang, H.; Jian, Z.; Shen, Y.; Li, C.; Wang, C.; Xie, A. A Simple Method To Synthesize Modified Fe_3O_4 for the Removal of Organic Pollutants on Water Surface. *Appl. Surf. Sci.* **2012**, *258*, 6326–6330.
15. Zhu, Q.; Tao, F.; Pan, Q. Fast and Selective Removal of Oils from Water Surface *via* Highly Hydrophobic Core-Shell Fe_2O_3@C Nanoparticles under Magnetic Field. *ACS Appl. Mater. Interfaces* **2010**, *2*, 3141–3146.
16. Chu, Y.; Pan, Q. Three-Dimensionally Macroporous Fe/C Nanocomposites as Highly Selective Oil-Absorption Materials. *ACS Appl. Mater. Interfaces* **2012**, *4*, 2420–2425.
17. Pyun, J. Nanocomposite Materials from Functional Polymers and Magnetic Colloids. *Polym. Rev.* **2007**, *47*, 231–263.
18. Wang, S.; Li, M.; Lu, Q. Filter Paper with Selective Absorption and Separation of Liquids that Differ in Surface Tension. *ACS Appl. Mater. Interfaces* **2010**, *2*, 677–683.
19. Feng, X. J.; Jiang, L. Design and Creation of Superwetting/Antiwetting Surfaces. *Adv. Mater.* **2006**, *18*, 3063–3078.
20. Dollhopf, R.; *Proposed Order for Recovery of Submerged Oil*; U.S. Environmental Protection Agency: Washington, D.C., **2012**.
21. Wang, P.; Shi, Q.; Shi, Y.; Clark, K. K.; Stucky, G. D.; Keller, A. A. Magnetic Permanently Confined Micelle Arrays for Treating Hydrophobic Organic Compound Contamination. *J. Am. Chem. Soc.* **2009**, *131*, 182–188.
22. Wu, A.; Ou, P.; Zeng, L. Biomedical Applications of Magnetic Nanoparticles. *Nano Brief Rep. Rev.* **2010**, *05*, 245–270.
23. Zeisberger, M.; Dutz, S.; Müller, R.; Hergt, R.; Matoussevitch, N.; Bönnemann, H. Metallic Cobalt Nanoparticles for Heating Applications. *J. Magn. Magn. Mater.* **2007**, *311*, 224–227.
24. O'Reilly, R. K.; Joralemon, M. J.; Hawker, C. J.; Wooley, K. L. Facile Syntheses of Surface-Functionalized Micelles and Shell Cross-Linked Nanoparticles. *J. Polym. Sci., Polym. Chem.* **2006**, *44*, 5203–5217.
25. Lin, L. Y.; Lee, N. S.; Zhu, J.; Nystrom, A. M.; Pochan, D. J.; Dorshow, R. B.; Wooley, K. L. Tuning Core *vs*. Shell Dimensions to Adjust the Performance of Nanoscopic Containers for the Loading and Release of Doxorubicin. *J. Controlled Release* **2011**, *152*, 37–48.
26. Sun, S.; Zeng, H.; Robinson, D. B.; Raoux, S.; Rice, P. M.; Wang, S. X.; Li, G. Monodisperse MFe_2O_4 (M = Fe, Co, Mn) Nanoparticles. *J. Am. Chem. Soc.* **2004**, *126*, 273–279.
27. Bao, N.; Shen, L.; Wang, Y.; Padhan, O.; Gupta, A. A Facile Thermolysis Route to Monodisperse Ferrite Nanocrystals. *J. Am. Chem. Soc.* **2007**, *129*, 12374–12375.
28. Davis, K. A.; Charleux, B.; Matyjaszewski, K. Preparation of Block Copolymers of Polystyrene and Poly (*t*-butyl acrylate) of Various Molecular Weights and Architectures by Atom Transfer Radical Polymerization. *J. Polym. Sci., Polym. Chem.* **2000**, *38*, 2274–2283.
29. Kim, B.; Qiu, J.; Wang, J.; Taton, T. A. Magnetomicelles: Composite Nanostructures from Magnetic Nanoparticles and Cross-Linked Amphiphilic Block Copolymers. *Nano Lett.* **2005**, *5*, 1987–1991.
30. Hickey, R. J.; Haynes, A. S.; Kikkawa, J. M.; Park, S. J. Controlling the Self-Assembly Structure of Magnetic Nanoparticles and Amphiphilic Block-Copolymers: From Micelles to Vesicles. *J. Am. Chem. Soc.* **2011**, *133*, 1517–1525.
31. Joralemon, M. J.; O'Reilly, R. K.; Hawker, C. J.; Wooley, K. L. Shell Click-Crosslinked (SCC) Nanoparticles: A New

Methodology for Synthesis and Orthogonal Functionalization. *J. Am. Chem. Soc.* **2005**, *127*, 16892–16899.
32. Huang, H.; Kowalewski, T.; Remsen, E. E.; Gertzmann, R.; Wooley, K. L. Hydrogel-Coated Glassy Nanospheres: A Novel Method for the Synthesis of Shell Cross-Linked Knedels. *J. Am. Chem. Soc.* **1997**, *119*, 11653–11659.
33. Lehr, B.; Bristol, S.; Possolo, A. *Oil Budget Calculator: Deepwater Horizon*; The Federal Interagency Solutions Group, Oil Budget Calculator Science and Engineering Team: Washington, D.C.; **2010**. http://www.restorethegulf.gov/sites/default/files/documents/pdf/OilBudgetCalc_-Full_HQ-Print_111110.pdf.
34. GPC Theory: Refractive Index Detectors; Malvern. http://www.malvern.com/labeng/technology/gel_permeation_chromatography_theory/refractive_index_detector_gpc_theory.htm.
35. Huang, T.; Brown, R.; Cong, R.; Yau, W.; Hazlitt, L.; deGroot, A. W. True" Concentration Determination Using a Concentration and Composition Sensitive Infrared Detector for Molecular Weight Characterization of Polyolefins. *Macromol. Symp.* **2012**, *312*, 20–26.
36. Usami, T.; Gotoh, Y.; Takayama, S. Determination of the Ring Concentration in Polyoctenamer. *Eur. Polym. J.* **1985**, *21*, 885–889.
37. Bajaj, H.; Sharma, V. K.; Kalonia, D. S. A High-Throughput Method for Detection of Protein Self-Association and Second Virial Coefficient Using Size-Exclusion Chromatography through Simultaneous Measurement of Concentration and Scattered Light Intensity. *Pharm. Res.* **2007**, *24*, 2071–2083.
38. Teas, C.; Kalligeros, S.; Zanikos, F.; Stournas, S.; Lois, E.; Anastopoulos, G. Investigation of the Effectiveness of Absorbent Materials in Oil Spills Clean Up. *Desalination* **2001**, *140*, 259–264.